Title

MEL-28/ELYS and CENP-C coordinately control outer kinetochore assembly and meiotic chromosome-microtubule interactions

Journal

Current Biology, 32(11)

ISSN

0960-9822

Authors

Hattersley, Neil
Schlientz, Aleesa J
Prevo, Bram
et al.

Publication Date

2022-06-01

DOI

10.1016/j.cub.2022.04.046

Peer reviewed

HHS Public Access

Author manuscript

Curr Biol. Author manuscript; available in PMC 2023 June 06.

Published in final edited form as:

Curr Biol. 2022 June 06; 32(11): 2563–2571.e4. doi:10.1016/j.cub.2022.04.046.

MEL-28/ELYS and CENP-C coordinately control outer kinetochore assembly and meiotic chromosome-microtubule interactions

Neil Hattersley[1,*],

Aleesa J. Schlientz[2,*],

Bram Prevo[1],

Karen Oegema[1,2],

Arshad Desai[1,2]

[1]Ludwig Institute for Cancer Research, San Diego Branch, La Jolla, CA 92093, USA

[2]Division of Biological Sciences & Department of Cellular & Molecular Medicine, University of California San Diego, La Jolla, CA 92093, USA

SUMMARY

During mitosis and meiosis in the majority of eukaryotes, centromeric chromatin comprised of CENP-A nucleosomes and their reader CENP-C recruits components of the outer kinetochore to build an interface with spindle microtubules[1, 2]. One exception is *C. elegans* oocyte meiosis, where outer kinetochore proteins form cup-like structures on chromosomes independently of centromeric chromatin[3]. Here we show that the nucleoporin MEL-28 (ortholog of human ELYS) and CENP-C^{HCP-4} act in parallel to recruit outer kinetochore components to oocyte meiotic chromosomes. Unexpectedly, co-inhibition of MEL-28 and CENP-C^{HCP-4} resulted in chromosomes being expelled from the meiotic spindle prior to anaphase onset, a more severe phenotype than what was observed following ablation of the outer kinetochore[4, 5]. This observation suggested that MEL-28 and the outer kinetochore independently link chromosomes to spindle microtubules. Consistent with this, the chromosome expulsion defect was observed following co-inhibition of MEL-28 and the microtubule-coupling KNL-1/MIS-12/NDC-80 (KMN) network of the outer kinetochore. Use of engineered mutants showed that MEL-28 acts in conjunction with the microtubule-binding NDC-80 complex to keep chromosomes within the oocyte meiotic spindle, and that this function

@: Corresponding author & Lead Contact: abdesai@ucsd.edu, Phone:(858)-534-9698, Fax: (858)-534-7750, Address: CMM-E Rm 3052, 9500 Gilman Dr, La Jolla, CA 92093-0653.

*co-first authors

AUTHOR CONTRIBUTIONS

N.H. and A.D. initiated the project; N.H. conducted the majority of experiments and prepared figure and text drafts; A.J.S. performed experimental analysis of MEL-28 truncations and of KLP-19, participated in manuscript and figure preparation, and helped prepare the revision; B.P. constructed the strain with fluorescently tagged KLP-19; K.O. provided feedback throughout the course of the project and K.O. and B.P. edited the manuscript.

DECLARATION OF INTERESTS

Neil Hattersley is currently an employee of AstraZeneca. The authors declare no competing financial interests.

likely involves the Y-complex of nucleoporins that associate with MEL-28; by contrast, the ability to dock protein phosphatase 1, shared by MEL-28 and KNL-1, is not involved. These results highlight nuclear pore-independent functions for a conserved nucleoporin and explain two unusual features of oocyte meiotic chromosome segregation in *C. elegans* – centromeric chromatin-independent outer kinetochore assembly, and dispensability of the outer kinetochore for constraining chromosomes in the acentrosomal meiotic spindle.

eTOC BLURB

C. elegans oocyte meiotic chromosomes assemble an outer kinetochore in the absence of centromeric chromatin. Hattersley *et al.* show that the nucleoporin MEL-28/ELYS is required for centromeric chromatin-independent kinetochore assembly. In addition, MEL-28 contributes to chromosome-spindle interactions independently of the outer kinetochore.

Keywords

nuclear pore; kinetochore; centromere; meiosis; ELYS; CENPC; CENPA; KMN network; NDC80; oocyte; spindle; *C. elegans*

RESULTS & DISCUSSION

During *C. elegans* oocyte meiosis, outer kinetochore proteins localize to cup-like structures on chromosomes and to linear elements that are in the spindle and throughout the oocyte[3, 4] (Figure 1A). By contrast, the centromeric chromatin component CENP-C^{HCP-4} localizes throughout chromatin (Figure 1A), and its depletion does not perturb the chromosomal localization of outer kinetochore components such as KNL-1, MIS-12 and NDC-80 complexes[3] (KMN network). Notably, during the first embryonic mitosis that occurs ~25 min after completion of oocyte meiosis, CENP-C^{HCP-4} co-localizes with outer kinetochore components and its depletion abolishes outer kinetochore assembly[6]. These observations indicate the existence of a CENP-C^{HCP-4}-independent mechanism acting during oocyte meiosis to recruit outer kinetochore proteins to the chromosome surface.

During oocyte meiosis, the nucleoporin MEL-28, the *C. elegans* ortholog of ELYS in vertebrates, plays a critical role independently of the nuclear pore[7]. Specifically, MEL-28 employs a conserved motif to localize protein phosphatase 1 (PP1) to the chromosome surface during anaphase, which is essential for anaphase chromosome separation[7]. PP1 docking by MEL-28 is also important for nuclear pore assembly and nuclear expansion during meiotic/mitotic exit[7], when MEL-28/ELYS associates with chromatin and recruits the conserved Y-complex of nucleoporins to initiate pore assembly[8]. Notably, during anaphase of *C. elegans* oocyte meiosis, MEL-28 acts independently of core Y-complex subunits[7].

Prior to anaphase I, MEL-28 exhibits chromosomal localization that is identical to outer kinetochore components, but its depletion does not prevent localization of outer kinetochore components such as KNL-3 or KNL-1[7] (Figure 1B). In addition, localization of MEL-28 to the chromosome surface is unaffected by depletion of CENP-C^{HCP-4} or of outer kinetochore scaffolds, such as KNL-3 or KNL-1[7] (Figure S1A). We therefore hypothesized that parallel

action of MEL-28 and CENP-C^{HCP-4} may account for the lack of effect of their individual inhibitions on outer kinetochore assembly. Consistent with this idea, when MEL-28 and CENP-C^{HCP-4} were co-inhibited, either by co-depletion using RNAi (Figure 1B) or by depletion of CENP-C^{HCP-4} at the restrictive temperature in the *mel-28(ax640)* temperature-sensitive (*ts*) mutant[9] (Figure 1C–E; Figure S1B), the bivalent oocyte chromosomes lacked outer kinetochore components on their surface; this result was observed by both immunofluorescence of endogenous outer kinetochore proteins and live imaging of *in situ* GFP-tagged KMN components (Figure 1B–E). In the double-inhibited oocytes, outer kinetochore KMN components formed large aggregates (Figure 1B,C,E), potentially due to coalescence of the linear elements. These results suggest that MEL-28 and CENP-C^{HCP-4} act in parallel to recruit components of the outer kinetochore to the surface of meiotic chromosomes and explain why perturbation of centromeric chromatin alone does not prevent outer kinetochore assembly.

The parallel action of CENP-C^{HCP-4} and MEL-28 in recruiting outer kinetochore components to the chromosome surface is surprising, given that CENP-C^{HCP-4} does not itself exhibit the cup-like localization pattern (Figure 1A). This observation suggests that only chromosome surface-localized CENP-C^{HCP-4} bound to CENP-A nucleosomes can associate with the KMN network. The oligomeric nature of the KMN network[10] may also contribute to restricting it to the chromosome surface. The mechanism by which MEL-28 is recruited to the chromosome surface to form cups independently of centromere/kinetochore components is at present not known.

While conducting live imaging of MEL-28 and CENP-C^{HCP-4} double-inhibited oocyte meiosis I, we observed chromosome alignment to be significantly defective (Figure 1B,C,E); by contrast, CENP-C^{HCP-4} depletion did not affect chromosome alignment or segregation[3] (Figure 1C) and MEL-28 inhibition did not affect events up to metaphase, although it prevented anaphase chromosome separation[7] (Figure 1C). To address if the severe chromosome alignment defect in the double-inhibited oocytes was a consequence of disrupting formation of the KMN-containing cup kinetochores, we imaged control, MEL-28 depleted, KNL-1 depleted, and MEL-28 and KNL-1 double-depleted oocyte meiosis I in a strain with fluorescently marked chromosomes and microtubules. If the observed defects were due to loss of outer kinetochore cups, then KNL-1 single depletion and the double KNL-1 and MEL-28 depletion should exhibit similar phenotypes. In control oocytes, the well-described pattern of acentrosomal bipolar spindle formation[11–13], perpendicular alignment of the spindle to the cell cortex by rotation[14], significant spindle shortening that occurs coincident with rotation[15], and eventual transition into anaphase[11, 13] was observed. While the single depletions exhibited phenotypes consistent with prior analysis[4, 7], MEL-28 and KNL-1 double-depletions exhibited significantly more severe defects than the individual depletions (Figure 2A,D). In the double-depletion, at the time of spindle shortening and rotation, chromosomes were expelled from the spindle core and were observed on the outside surface of the collapsed spindle (Figure 2A), a configuration that we refer to as the “satellite” phenotype, based on its visual appearance. The satellite phenotype was never observed in control embryos or in the individual MEL-28 and KNL-1 inhibitions but was similar to defects observed in CENP-C^{HCP-4} and MEL-28 double-inhibited oocytes (Figure 2B,D).We note that the CENP-C^{HCP-4} and MEL-28 double depletion resulted

in a qualitatively more severe phenotype than the KNL-1 and MEL-28 double depletion (4/9 oocytes had bivalents that appeared detached from the spindle in the former versus 0/13 in the latter; the detached bivalents eventually reassociated with the spindle (*not shown*)). One potential explanation for increased severity may be the presence of large KMN aggregates in the spindle region in the CENP-C^{HCP-4} and MEL-28 double depletion (Figure 1B,C,E). Based on the phenotypic difference between the MEL-28 and KNL-1 double depletion versus the KNL-1 single depletion, we conclude that MEL-28 provides a function independent of KMN network recruitment to the chromosome surface that helps retain chromosomes in the meiotic spindle.

We next addressed how the satellite phenotype developed in MEL-28 and KNL-1 double-inhibited oocytes. Imaging of *in situ*-tagged fluorescent fusion of ASPM-1[16, 17], a marker for the acentrosomal spindle poles in oocyte spindles[14], indicated that spindles exhibiting the satellite phenotype were bipolar (Figure S2), which is consistent with early stages of spindle assembly not being significantly perturbed in the double-inhibited state. The satellite phenotype observed in MEL-28 and KNL-1 double-inhibited oocytes emerged at the time of spindle shortening and rotation[14, 15], two events that position the meiotic spindle adjacent and perpendicular to the cell cortex prior to anaphase onset and polar body extrusion. Both spindle shortening and rotation require activation of the anaphase promoting complex/cyclosome (APC/C)[18–20], the E3 ubiquitin ligase that degrades securin and cyclin B to separate homologous chromosomes and transition the zygote from meiosis I to meiosis II. We therefore tested if APC/C-dependent spindle shortening was required for the satellite phenotype in the double MEL-28 and KNL-1 inhibition. For this purpose, we conducted double RNAi of MEL-28 and KNL-1 in a temperature-sensitive mutant of the APC/C subunit APC4^{EMB-30} (Figure 2C,D). Inhibition of the APC/C prevented the satellite phenotype, indicating that the expulsion of chromosomes from the spindle core occurs during the shortening of the spindle prior to anaphase onset (Figure 2C,D). We note that, in the double-inhibition, expelled chromosomes remained associated with the surface of the collapsed spindle (e.g. Figure 2A), potentially via microtubule-interacting components that localize to their mid-bivalent region, such as the chromokinesin KLP-19 (Figure S1C)[4]. Thus, while MEL-28 and CENP-C^{HCP-4} act in parallel to recruit outer kinetochore components, MEL-28 makes a functional contribution independently of the outer kinetochore to the retention of chromosomes within the oocyte spindle during its dynamic transition prior to anaphase onset.

As both MEL-28 and KNL-1 dock protein phosphatase 1[7, 21] (PP1), we first tested if PP1 recruitment was the common property whose loss resulted in the satellite phenotype. For this purpose, we took advantage of a previously developed RNAi-based KNL-1 replacement system, in which endogenous KNL-1 is depleted in oocytes containing either a wild-type or PP1-docking deficient RNAi-resistant *knl-1* transgene[22]. Expression of either wild-type or PP1-docking deficient KNL-1 rescued the satellite phenotype in MEL-28 and KNL-1 double-depleted oocytes (Figure 3A,D). Thus, PP1 docking is not the activity provided by MEL-28 and KNL-1 that underlies the satellite phenotype observed in MEL-28 and KNL-1 double-inhibited oocytes. In KNL-1-depleted meiosis I, the majority of outer kinetochore components are prevented from localizing to the chromosome surface[4]. To assess if the satellite phenotype observed in MEL-28 and KNL-1 double-inhibited oocytes was specific

to removal of KNL-1 or due to its central role in outer kinetochore assembly, we conducted double inhibition analyses of MEL-28 with the KNL-3 subunit of the MIS-12 complex, the key microtubule-binding NDC-80 subunit of the KMN network, and the ROD-1 subunit of the Rod/Zwilch/Zw10 (RZZ) complex, whose recruitment depends on the KMN network and which, in turn, recruits the molecular motor dynein[4, 23]. We found that both KNL-3 and NDC-80 depletion resulted in a satellite phenotype when combined with MEL-28 inhibition (Figure 3B,D); by contrast, ROD-1 depletion did not (Figure 3B,D).

The expulsion of chromosomes during meiosis I spindle shortening when MEL-28 was inhibited together with either KNL-1, KNL-3 or NDC-80 suggested that the expulsion may be due to loss of chromosome-microtubule interactions independently mediated by MEL-28 and the KMN network on the chromosome surface. MEL-28 associates with the Y-complex of nucleoporins[24], whose subunits also localize to meiotic kinetochore cups[7], however the direct/indirect association of MEL-28 and Y-complex subunits with microtubules are not well understood[25, 26]. By contrast, microtubule interaction of the KMN network, mediated by the NDC-80 subunit of the NDC-80 complex, has been characterized at a detailed structural level[27–30]. We therefore focused on NDC-80 to address whether disruption of microtubule interactions, independently provided by MEL-28 and the KMN network, was the reason for the satellite phenotype. For this purpose, we employed a previously developed RNAi-based NDC-80 replacement system, in which endogenous NDC-80 is replaced by either wild-type NDC-80 or a mutant form, referred to as CH^{mut}, in which 6 structure-guided amino acid mutations were engineered into the N-terminal calponin homology (CH) domain to specifically disrupt NDC-80's docking onto the microtubule lattice[27] (Figure 3C). MEL-28 inhibition in the presence of wild-type NDC-80 did not result in a satellite phenotype (Figure 3C,D); instead the MEL-28 loss-of-function phenotype, characterized by normal chromosome alignment and spindle assembly through end of metaphase but failure of anaphase chromosome separation, was observed. By contrast, MEL-28 inhibition in the presence of the CH^{mut} NDC-80 resulted in a satellite phenotype (Figure 3C,D). Thus, selective inhibition of the key microtubule-interacting surface in the KMN network indicates that the NDC-80 subunit of the KMN network acts coordinately with MEL-28 to link meiotic chromosomes to spindle microtubules. These parallel activities provided by MEL-28 and KMN microtubule binding are necessary to keep the chromosomes within the meiotic spindle as it shortens prior to anaphase onset.

We next addressed if MEL-28 accumulation on kinetochore cups is important for its functions in meiotic kinetochore assembly and chromosome-spindle interactions. For this purpose, we focused on identifying a mutant of MEL-28 that perturbs its cup localization but does not prevent its other functions. Prior analysis of ELYS, the vertebrate ortholog of MEL-28, identified two conserved structured domains in its N-terminal half: a beta propeller followed by an alpha helical solenoid[31] (Figure 4A); these structured domains mediate ELYS's interaction with the Y-complex of nucleoporins[31]. The C-terminal half of MEL-28 is predicted to be largely unstructured and contains a PP1 binding site immediately after the structured domains and two putative AT hooks near the C-terminal end (Figure 4A). In ELYS, C-terminal AT hooks are implicated in DNA and nucleosome binding[32, 33]; the AT hook-containing region of ELYS has also been reported to bind to microtubules[25]. We employed a previously developed MEL-28 replacement system to compare wild-type

(WT) GFP::MEL-28 to a truncation (ΔCT) that retains the structured domains and the PP1 binding site but deletes the C-terminal 225 amino acids that contain the putative AT hooks. Notably ΔCT MEL-28 supports the function of MEL-28 in meiosis I anaphase chromosome segregation[7], indicating it does not lead to loss of MEL-28 function. Analysis of the localization of WT and ΔCT MEL-28 GFP fusions revealed that, in contrast to the WT, ΔCT MEL-28 exhibited very weak localization to kinetochore cups during prometaphase (Figure 4A); however, ΔCT MEL-28 exhibited robust localization to the spindle in metaphase (Figure 4A) and around chromosomes in anaphase (*not shown*), consistent with its ability to support the PP1 recruitment-dependent anaphase segregation function of MEL-28[7]. Thus, the C-terminal 225 amino acids of MEL-28 are important for its localization to kinetochore cups, leading to the prediction that ΔCT MEL-28 should not support the functions of MEL-28 in meiotic kinetochore assembly and chromosome-spindle interactions.

To assess the phenotypic consequences of the C-terminal deletion of MEL-28, we depleted CENP-C^{HCP-4} and inactivated endogenous MEL-28 in the presence of transgene-encoded untagged WT or ΔCT MEL-28. Under these conditions, transgene-encoded WT MEL-28 supported robust kinetochore cup assembly, as assessed by localization of KNL-3, whereas ΔCT MEL-28 was severely compromised (Figure 4B). In addition, CENP-C^{HCP-4} depletion in ΔCT MEL-28 resulted in a penetrant satellite phenotype; by contrast, no satellite phenotype was observed with WT MEL-28 (Figure 4C). These data indicate that elements in the C-terminal 225 amino acids of MEL-28 are critical for its localization to the chromosome surface and for both of its pre-anaphase functions: supporting centromeric chromatin-independent meiotic kinetochore assembly and acting in parallel to the outer kinetochore to constrain chromosomes in the acentrosomal meiotic spindle.

Finally, we assessed if the synergy between MEL-28 and KMN network inhibition was specific to MEL-28 or was also observed with core Y-complex nucleoporins that localize to kinetochore cups. For this purpose, we focused on NUP160^{NPP-6}, whose depletion results in identical nuclear assembly defects as depletion of MEL-28[34]; based on work in other systems, NUP160^{NPP-6} is thought to form the primary binding interface between the structured N-terminal half of MEL-28/ELYS & the Y-complex[35]. NUP160^{NPP-6} inhibition on its own did not impact meiotic chromosome segregation or result in a satellite phenotype ([7] & Figure S3). However, double depletion of NUP160^{NPP-6} and KNL-1 resulted in a penetrant satellite phenotype, similar to what was observed for MEL-28 and KNL-1 co-depletion (Figure 4D; Figure S3). Thus, unlike the meiotic anaphase promotion function, which is intrinsic to MEL-28, chromosome retention in the oocyte spindle involves the MEL-28 associated core Y-complex of nucleoporins.

In conclusion, we show here that the nucleoporin MEL-28, primarily studied for its role in nuclear pore formation during mitotic exit[24, 33, 36], plays a critical role in both outer kinetochore assembly and chromosome-spindle interactions during oocyte meiosis in *C. elegans* (Figure 4E). These activities precede the role of MEL-28 in meiotic anaphase, which involves its ability to directly recruit PP1[7]. While the meiotic anaphase function is intrinsic to MEL-28, the roles ascribed here potentially involve the MEL-28-associated Y-complex (Figure 4E). These results collectively highlight nuclear pore complex-independent functions for conserved nucleoporins and explain two puzzling features of oocyte meiosis

I in *C. elegans*: why centromeric chromatin removal does not affect localization of outer kinetochore components and why loss of the outer kinetochore does not have a greater effect on chromosome-spindle interactions. We note that centromeric chromatin-independent recruitment of KMN network components to chromosomes has been observed in holocentric insects and in an early-diverging fungal clade with localized centromeres[37, 38]; unlike *C. elegans*, which employs a CENP-A-based kinetochore for mitotic chromosome segregation, CENP-A and CENP-C have been entirely lost in these species. In the best-studied holocentric lepidopteran insect species, *Bombyx mori*, a protein related to CENP-T mediates centromeric chromatin-independent kinetochore assembly[39]. Our analysis of MEL-28 as a distinct factor acting independently of centromeric chromatin raises a number of questions that will need to be addressed in future work, including how MEL-28 and its associated Y-complex get recruited to the surface of meiotic chromosomes, how they interface with the outer kinetochore KMN network, and how they, either directly or indirectly, help keep meiotic chromosomes inside the oocyte spindle as it shortens prior to anaphase onset (Figure 4E). It will also be interesting to explore why this set of nuclear pore complex components are being employed in this entirely distinct biological context.

STAR METHODS

RESOURCE AVAILABILITY

Lead contact—Further information and requests for resources and reagents should be directed to and will be fulfilled by the lead contact, Arshad Desai (abdesai@ucsd.edu).

Materials availability—All unique/stable reagents generated in this study are available from the Lead Contact without restriction.

Data and code availability

- All data reported in this paper will be shared by the lead contact upon request.
- This paper does not report original code.
- Any additional information required to reanalyze the data reported in this paper is available from the lead contact upon request.

EXPERIMENTAL MODEL AND SUBJECT DETAILS

C. elegans *Strains*—*C. elegans* strains (see Key Resources Table) were maintained using standard methods at either 16°C (temperature sensitive strains) or 20°C (all other strains). In brief, worms were maintained on standard nematode growth medium plates seeded with OP50–1 *E. coli*. Temperature sensitive strains were used at either 16°C (*permissive temperature*) or were shifted to 25–26°C for four hours prior to use (*restrictive temperature*).

METHOD DETAILS

RNA-interference—Double-stranded RNAs (dsRNAs) were generated using the oligos listed in the Key Resources Table, which were used to PCR amplify regions from genomic DNA or cDNA. PCR reactions served as templates for *in vitro* single-stranded transcription reactions (MEGAscript kit, Ambion); transcript products were purified using a MEGAclear

kit (Ambion). Eluted RNA from T7 and T3 transcription reactions were mixed equally in 3x soaking buffer (32.7 mM NNa2HP04, 16.5 mM KH2PO4, 6.3 mM KCl, and 14.1 mM NH4Cl), and annealed (68°C for 10 minutes followed by 37°C for 30 minutes). Following injection of dsRNA into L4 stage worms, imaging was performed 40–44 hours for strains maintained at 20°C or 48–52 hours for strains maintained at 16°C.

Immunostaining—For immunofluorescence, uncoated slides were coated with subbing solution[7] (100mL water, 0.4g gelatin, 0.04g chromalum, 100mg poly-l-lysine; filter sterilized) by heating the solution to 50°C, immersing the slides, and drying overnight. 12–15 gravid adult hermaphrodites were dissected into 3.2μl of 0.8x egg salts made fresh from an egg salt solution (1x solution = 118 mM NaCl, 40 mM KCl, 3.4 mM $MgCl_2$, 3.4 mM $CaCl_2$ and 5mM HEPES (pH 7.4)) on a slide coated with subbing solution before covering with a 12×12mm coverslip, allowing capillary action to extrude embryos and oocytes, and immersing in liquid nitrogen. For the *mel-28*^{ts} strain, worms were kept on a low-temperature surface before dissection (1–2 minutes) and liquid nitrogen immersion (Figure 1D). After removal from liquid nitrogen, coverslips were quickly removed, and slides fixed in −20°C methanol for 10–15 minutes. Slides were then washed with PBS, dried with a Kimwipe (except for area containing embryos/oocytes), and the slide region containing the oocytes was circled with a PAP pen. Oocytes were then blocked with AbDil (PBS, 0.1% Triton X-100, 0.1%NaN_3, and 2% BSA) and incubated with directly-labeled primary antibodies[6, 40, 41]. Samples were washed with AbDil followed by staining with Hoechst. Samples were mounted in an antifade reagent, overlaid with a coverslip, and sealed with nail polish.

Imaging and Analysis—Live-imaging was performed using either a spinning disk confocal microscope (Revolution XD Confocal System; Andor Technology), or a Delta-Vision wide-field microscope (Applied Precision). The spinning disk confocal system was equipped with a CSU-10 (Yokogawa) spinning disk, 60× 1.4NA Plan Apochromat and 100× 1.4NA Plan Apochromat oil objective lenses, solid-state 100mW lasers, and an iXon DV887 EMCCD camera (Andor) mounted on a TE2000-E (Nikon) microscope base. The wide-field microscope was equipped with a CCD camera (CoolSNAP; Roper Scientific) and a 100× 1.35NA U Plan Apochromat oil objective lens (Olympus) mounted on an IX70 Olympus microscope base.

Live oocytes were imaged by dissecting oocytes from gravid adult hermaphrodites in 0.8x egg salts made fresh from an egg salt solution (1x solution = 118 mM NaCl, 40 mM KCl, 3.4 mM $MgCl_2$, 3.4 mM $CaCl_2$ and 5mM HEPES (pH 7.4)). Fertilized oocytes in prometaphase I were mounted in a microdevice designed for *C. elegans* embryos[42]. Live-imaging of ΔCT MEL-28 and GFP::KLP-19 was performed by dissecting gravid adult hermaphrodites in 1X egg salt solution and mounting on a 2% agarose pad made with egg salt solution. Fixed and immunostained oocytes were imaged using Delta-Vision wide-field microscope (Applied Precision) as above.

All images and movies were processed, scaled, and analyzed using ImageJ/Fiji[43] (National Institutes of Health). Metaphase I (0s) was defined as the first frame after the rotation that orients the spindle axis to be perpendicular to the cortex was completed.

Assessment of Satellite Phenotype—The satellite phenotype was assessed during late prometaphase and metaphase in live imaging datasets where both chromosomes and spindle microtubules were fluorescently labeled. An oocyte was scored as having the satellite phenotype if one or more chromosomes were consistently observed on the outer surface of the spindle microtubule mass. A spindle was determined to have detached bivalents if one or more chromosomes were observed disjoined from the spindle microtubule mass.

In situ *GFP Tagging of KLP-19*—Endogenous KLP-19 (Y43F4B.6) was tagged with GFP using CRISPR/Cas9 editing[44]. Adult N2 worm germlines were injected with a plasmid encoding P*eft-3*::Cas9 and a single guide RNA (5'-ACCATTCATAGGCCTAGCA-3') (pDD162, 40ng/μl), a repair template (described below, 50ng/μl), and three plasmids for negative selection of extrachromosomal array-containing animals via fluorescence screening[45] (pCFJ90 (2.5ng/μl), pCFJ104 (5ng/μl), and pGH8 (10ng/μl)). The repair template consisted of a plasmid that included a 489bp left homology arm comprised of the *klp-19* 5' UTR preceding the GFP and linker (GGRAGSG) sequences, and a 1665bp right homology arm comprised of the *klp-19* coding sequence. Genotyping to confirm *in situ* tagging was conducted by PCR spanning both homology regions.

QUANTIFICATION AND STATISTICAL ANALYSIS

Graphs displaying the frequency of oocyte meiotic spindles with the specified phenotype were generated using GraphPad Prism. This paper does not report any statistical analysis.

Supplementary Material

Refer to Web version on PubMed Central for supplementary material.

ACKNOWLEDGMENTS

We are very grateful to Hala Fahs and Kris Gunsalus (NYU, Abu Dhabi) for alerting us to and sharing the *mel-28(ax640)* temperature-sensitive allele. We thank members of the Oegema and Desai labs for helpful discussions. This work was supported by a grant from the NIH to A.D. (GM074215). A.D. and K.O. received salary support from the Ludwig Institute for Cancer Research.

References

1. Cheeseman IM, Desai A. Molecular architecture of the kinetochore-microtubule interface. Nat Rev Mol Cell Biol. 2008;9(1):33–46. [PubMed: 18097444]
2. Santaguida S, Musacchio A. The life and miracles of kinetochores. EMBO J. 2009;28(17):2511–31. [PubMed: 19629042]
3. Monen J, Maddox PS, Hyndman F, Oegema K, Desai A. Differential role of CENP-A in the segregation of holocentric C. elegans chromosomes during meiosis and mitosis. Nat Cell Biol. 2005;7(12):1248–55. [PubMed: 16273096]
4. Dumont J, Oegema K, Desai A. A kinetochore-independent mechanism drives anaphase chromosome separation during acentrosomal meiosis. Nat Cell Biol. 2010;12(9):894–901. [PubMed: 20729837]
5. Danlasky BM, Panzica MT, McNally KP, Vargas E, Bailey C, Li W, et al. Evidence for anaphase pulling forces during C. elegans meiosis. J Cell Biol. 2020;219(12).
6. Cheeseman IM, Niessen S, Anderson S, Hyndman F, Yates JR 3rd, Oegema K, et al. A conserved protein network controls assembly of the outer kinetochore and its ability to sustain tension. Genes Dev. 2004;18(18):2255–68. [PubMed: 15371340]

7. Hattersley N, Cheerambathur D, Moyle M, Stefanutti M, Richardson A, Lee KY, et al. A Nucleoporin Docks Protein Phosphatase 1 to Direct Meiotic Chromosome Segregation and Nuclear Assembly. Dev Cell. 2016;38(5):463–77. [PubMed: 27623381]
8. Schellhaus AK, De Magistris P, Antonin W. Nuclear Reformation at the End of Mitosis. J Mol Biol. 2016;428(10 Pt A):1962–85. [PubMed: 26423234]
9. Asencio C, Davidson IF, Santarella-Mellwig R, Ly-Hartig TB, Mall M, Wallenfang MR, et al. Coordination of kinase and phosphatase activities by Lem4 enables nuclear envelope reassembly during mitosis. Cell. 2012;150(1):122–35. [PubMed: 22770216]
10. Kern DM, Kim T, Rigney M, Hattersley N, Desai A, Cheeseman IM. The outer kinetochore protein KNL-1 contains a defined oligomerization domain in nematodes. Mol Biol Cell. 2015;26(2):229–37. [PubMed: 25411336]
11. Mullen TJ, Davis-Roca AC, Wignall SM. Spindle assembly and chromosome dynamics during oocyte meiosis. Curr Opin Cell Biol. 2019;60:53–9. [PubMed: 31082633]
12. Severson AF, von Dassow G, Bowerman B. Oocyte Meiotic Spindle Assembly and Function. Curr Top Dev Biol. 2016;116:65–98. [PubMed: 26970614]
13. Dumont J, Desai A. Acentrosomal spindle assembly and chromosome segregation during oocyte meiosis. Trends Cell Biol. 2012;22(5):241–9. [PubMed: 22480579]
14. van der Voet M, Berends CW, Perreault A, Nguyen-Ngoc T, Gonczy P, Vidal M, et al. NuMA-related LIN-5, ASPM-1, calmodulin and dynein promote meiotic spindle rotation independently of cortical LIN-5/GPR/Galpha. Nat Cell Biol. 2009;11(3):269–77. [PubMed: 19219036]
15. Vargas E, McNally KP, Cortes DB, Panzica MT, Danlasky BM, Li Q, et al. Spherical spindle shape promotes perpendicular cortical orientation by preventing isometric cortical pulling on both spindle poles during C. elegans female meiosis. Development. 2019;146(20).
16. Connolly AA, Sugioka K, Chuang CH, Lowry JB, Bowerman B. KLP-7 acts through the Ndc80 complex to limit pole number in C. elegans oocyte meiotic spindle assembly. J Cell Biol. 2015;210(6):917–32. [PubMed: 26370499]
17. McNally KP, Panzica MT, Kim T, Cortes DB, McNally FJ. A novel chromosome segregation mechanism during female meiosis. Mol Biol Cell. 2016;27(16):2576–89. [PubMed: 27335123]
18. Furuta T, Tuck S, Kirchner J, Koch B, Auty R, Kitagawa R, et al. EMB-30: an APC4 homologue required for metaphase-to-anaphase transitions during meiosis and mitosis in Caenorhabditis elegans. Mol Biol Cell. 2000;11(4):1401–19. [PubMed: 10749938]
19. Verlhac MH, Terret ME, Pintard L. Control of the oocyte-to-embryo transition by the ubiquitin-proteolytic system in mouse and C. elegans. Curr Opin Cell Biol. 2010;22(6):758–63. [PubMed: 20943362]
20. Golden A, Sadler PL, Wallenfang MR, Schumacher JM, Hamill DR, Bates G, et al. Metaphase to anaphase (mat) transition-defective mutants in Caenorhabditis elegans. J Cell Biol. 2000;151(7):1469–82. [PubMed: 11134076]
21. Rosenberg JS, Cross FR, Funabiki H. KNL1/Spc105 recruits PP1 to silence the spindle assembly checkpoint. Curr Biol. 2011;21(11):942–7. [PubMed: 21640906]
22. Espeut J, Cheerambathur DK, Krenning L, Oegema K, Desai A. Microtubule binding by KNL-1 contributes to spindle checkpoint silencing at the kinetochore. J Cell Biol. 2012;196(4):469–82. [PubMed: 22331849]
23. Gassmann R, Essex A, Hu JS, Maddox PS, Motegi F, Sugimoto A, et al. A new mechanism controlling kinetochore-microtubule interactions revealed by comparison of two dynein-targeting components: SPDL-1 and the Rod/Zwilch/Zw10 complex. Genes Dev. 2008;22(17):2385–99. [PubMed: 18765790]
24. Galy V, Askjaer P, Franz C, Lopez-Iglesias C, Mattaj IW. MEL-28, a novel nuclear-envelope and kinetochore protein essential for zygotic nuclear-envelope assembly in C. elegans. Curr Biol. 2006;16(17):1748–56. [PubMed: 16950114]
25. Yokoyama H, Koch B, Walczak R, Ciray-Duygu F, Gonzalez-Sanchez JC, Devos DP, et al. The nucleoporin MEL-28 promotes RanGTP-dependent gamma-tubulin recruitment and microtubule nucleation in mitotic spindle formation. Nat Commun. 2014;5:3270. [PubMed: 24509916]

26. Mishra RK, Chakraborty P, Arnaoutov A, Fontoura BM, Dasso M. The Nup107–160 complex and gamma-TuRC regulate microtubule polymerization at kinetochores. Nat Cell Biol. 2010;12(2):164–9. [PubMed: 20081840]
27. Cheerambathur DK, Prevo B, Hattersley N, Lewellyn L, Corbett KD, Oegema K, et al. Dephosphorylation of the Ndc80 Tail Stabilizes Kinetochore-Microtubule Attachments via the Ska Complex. Dev Cell. 2017;41(4):424–37 e4. [PubMed: 28535376]
28. Ciferri C, Pasqualato S, Screpanti E, Varetti G, Santaguida S, Dos Reis G, et al. Implications for kinetochore-microtubule attachment from the structure of an engineered Ndc80 complex. Cell. 2008;133(3):427–39. [PubMed: 18455984]
29. Tooley JG, Miller SA, Stukenberg PT. The Ndc80 complex uses a tripartite attachment point to couple microtubule depolymerization to chromosome movement. Mol Biol Cell. 2011;22(8):1217–26. [PubMed: 21325630]
30. Alushin GM, Ramey VH, Pasqualato S, Ball DA, Grigorieff N, Musacchio A, et al. The Ndc80 kinetochore complex forms oligomeric arrays along microtubules. Nature. 2010;467(7317):805–10. [PubMed: 20944740]
31. Bilokapic S, Schwartz TU. Structural and functional studies of the 252 kDa nucleoporin ELYS reveal distinct roles for its three tethered domains. Structure. 2013;21(4):572–80. [PubMed: 23499022]
32. Zierhut C, Jenness C, Kimura H, Funabiki H. Nucleosomal regulation of chromatin composition and nuclear assembly revealed by histone depletion. Nat Struct Mol Biol. 2014;21(7):617–25. [PubMed: 24952593]
33. Rasala BA, Ramos C, Harel A, Forbes DJ. Capture of AT-rich chromatin by ELYS recruits POM121 and NDC1 to initiate nuclear pore assembly. Mol Biol Cell. 2008;19(9):3982–96. [PubMed: 18596237]
34. Galy V, Mattaj IW, Askjaer P. Caenorhabditis elegans nucleoporins Nup93 and Nup205 determine the limit of nuclear pore complex size exclusion in vivo. Mol Biol Cell. 2003;14(12):5104–15. [PubMed: 12937276]
35. Bilokapic S, Schwartz TU. Molecular basis for Nup37 and ELY5/ELYS recruitment to the nuclear pore complex. Proc Natl Acad Sci U S A. 2012;109(38):15241–6. [PubMed: 22955883]
36. Doucet CM, Talamas JA, Hetzer MW. Cell cycle-dependent differences in nuclear pore complex assembly in metazoa. Cell. 2010;141(6):1030–41. [PubMed: 20550937]
37. Drinnenberg IA, deYoung D, Henikoff S, Malik HS. Recurrent loss of CenH3 is associated with independent transitions to holocentricity in insects. Elife. 2014;3.
38. Navarro-Mendoza MI, Perez-Arques C, Panchal S, Nicolas FE, Mondo SJ, Ganguly P, et al. Early Diverging Fungus Mucor circinelloides Lacks Centromeric Histone CENP-A and Displays a Mosaic of Point and Regional Centromeres. Curr Biol. 2019;29(22):3791–802 e6. [PubMed: 31679929]
39. Cortes-Silva N, Ulmer J, Kiuchi T, Hsieh E, Cornilleau G, Ladid I, et al. CenH3-Independent Kinetochore Assembly in Lepidoptera Requires CCAN, Including CENP-T. Curr Biol. 2020;30(4):561–72 e10. [PubMed: 32032508]
40. Desai A, Rybina S, Muller-Reichert T, Shevchenko A, Shevchenko A, Hyman A, et al. KNL-1 directs assembly of the microtubule-binding interface of the kinetochore in C. elegans. Genes Dev. 2003;17(19):2421–35. [PubMed: 14522947]
41. Oegema K, Desai A, Rybina S, Kirkham M, Hyman AA. Functional analysis of kinetochore assembly in Caenorhabditis elegans. J Cell Biol. 2001;153(6):1209–26. [PubMed: 11402065]
42. Carvalho A, Olson SK, Gutierrez E, Zhang K, Noble LB, Zanin E, et al. Acute drug treatment in the early C. elegans embryo. PLoS One. 2011;6(9):e24656. [PubMed: 21935434]
43. Schindelin J, Arganda-Carreras I, Frise E, Kaynig V, Longair M, Pietzsch T, et al. Fiji: an open-source platform for biological-image analysis. Nat Methods. 2012;9(7):676–82. [PubMed: 22743772]
44. Dickinson DJ, Ward JD, Reiner DJ, Goldstein B. Engineering the Caenorhabditis elegans genome using Cas9-triggered homologous recombination. Nat Methods. 2013;10(10):1028–34. [PubMed: 23995389]

45. Frokjaer-Jensen C, Davis MW, Hopkins CE, Newman BJ, Thummel JM, Olesen SP, et al. Single-copy insertion of transgenes in Caenorhabditis elegans. Nat Genet. 2008;40(11):1375–83. [PubMed: 18953339]

HIGHLIGHTS

- *C. elegans* oocytes assemble a centromeric chromatin-independent kinetochore
- A nucleoporin directs centromeric chromatin-independent kinetochore assembly
- Nucleoporins also promote spindle interactions independently of the kinetochore
- Conserved nucleoporins act to ensure proper meiotic chromosome segregation

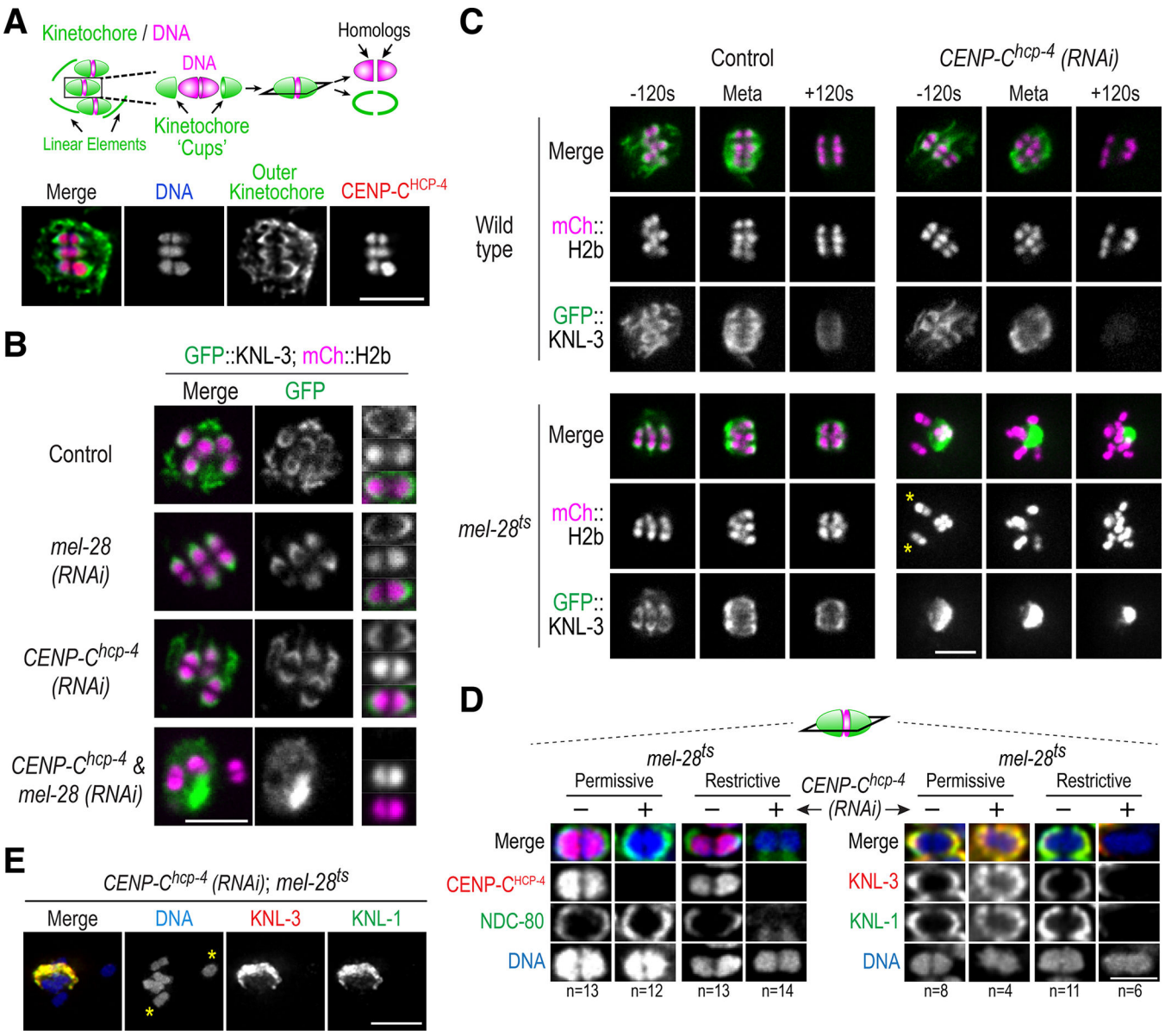

Figure 1. MEL-28 and CENP-C^{HCP-4} act in parallel to recruit outer kinetochore components to the surface of oocyte meiotic chromosomes.

(A) (*top*) Schematic of kinetochore protein organization in oocyte meiotic spindles. (*bottom*) Immunofluorescence image of an outer kinetochore component (KNL-3) and the centromeric chromatin component CENP-C^{HCP-4}. Scale bar, 5 μm. **(B)** Images of the outer kinetochore marker KNL-3 and chromosomes labeled with a fluorescent histone fusion for the indicated conditions. Panels to the right show KNL-3 (*top*), chromatin (*middle*) and the merge (*bottom*) for a single chromosome. *n* refers to number of oocytes imaged per condition. Scale bar, 5 μm. **(C)** Images from timelapse sequences monitoring chromosomes and the outer kinetochore component KNL-3 for the indicated conditions. Yellow asterisks indicate dispersed individual bivalent chromosomes that lack KNL-3 signal. For details on the *mel-28*^{ts} allele, see Figure S1B; all mel-28^{ts} analysis was conducted at the restrictive temperature of 25–26°C, unless noted otherwise. *n* refers to number of oocytes imaged per

condition. Scale bar, 5 μm. **(D) & (E)** Immunofluorescence analysis of the outer kinetochore components KNL3 and KNL-1 in the indicated condition. In (*D*), individual chromosomes are shown; the permissive temperature was 16°C and the restrictive temperature 25°C. *n* refers to number of fixed meiotic oocytes imaged per condition. In (*E*), the entire oocyte meiotic spindle region of one oocyte is shown. Yellow asterisks mark dispersed chromosomes of the type shown in (*D*). Scale bars, 2 μm (*D*) and 5 μm (*E*). Figure S1 provides additional related data, as referenced in the text.

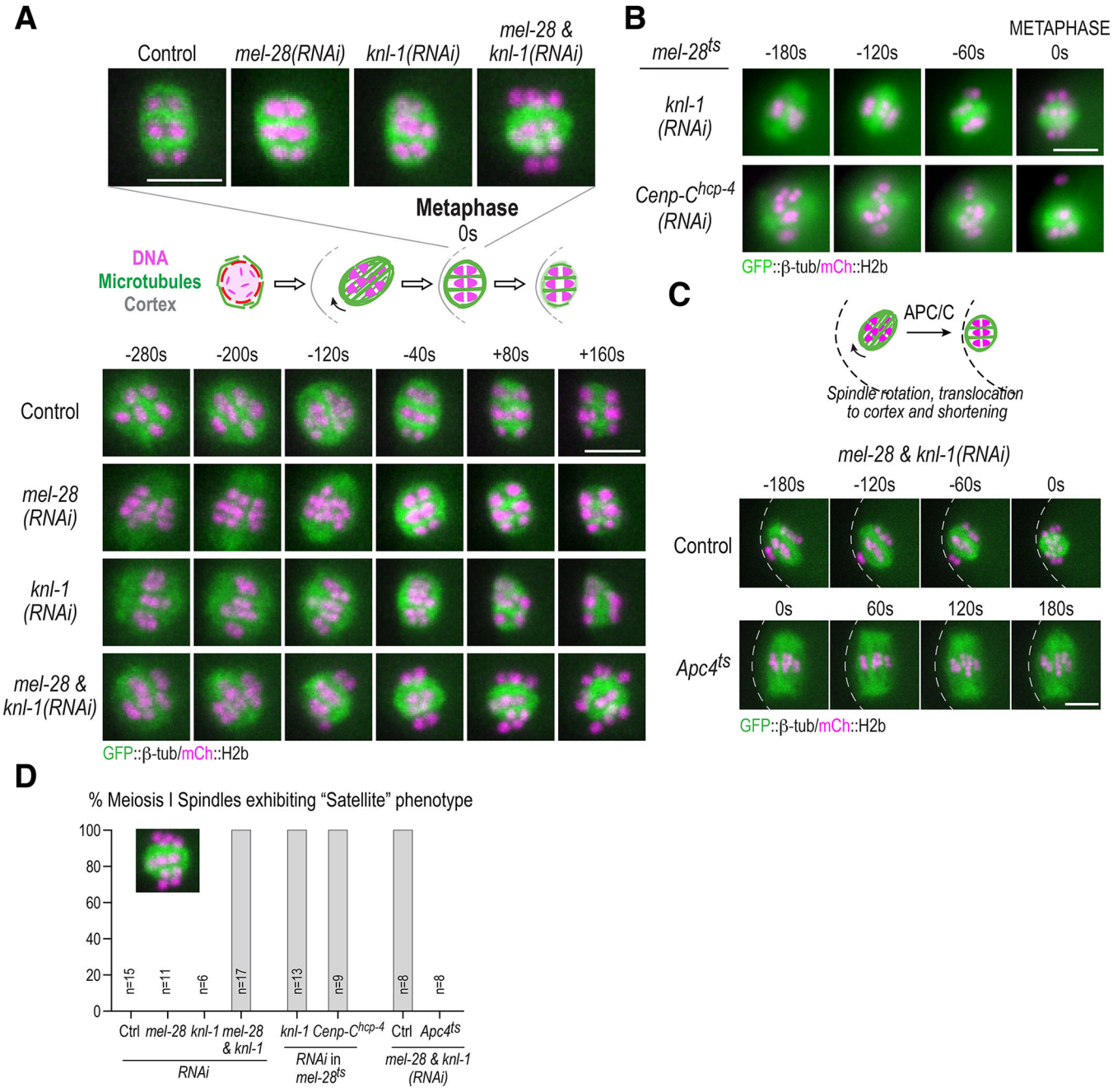

Figure 2. MEL-28 acts coordinately with the outer kinetochore to retain chromosomes in the spindle during its APC/C-dependent pre-anaphase shortening phase.

(A)(A) & (B) Images form timelapse sequences of the indicated conditions in a strain with fluorescently marked chromosomes and microtubules. Row above in (*A*) shows metaphase stage spindles from the sequences shown below. The double MEL-28 and KNL-1 inhibition exhibits a "satellite" phenotype with chromosomes on the outside of the spindle. Data supporting that the meiotic spindles under the conditions shown in Figure 2A are bipolar is shown in Figure S2. **(C)** (*top*) Schematic indicating APC/C activation-dependent spindle rotation and shortening. (*bottom*) Images of spindle and chromosome dynamics following

double depletion of MEL-28 and KNL-1 in a control strain and a strain with a temperature-sensitive mutation in *Apc4/emb-30*; both strains were filmed at the restrictive temperature of 25°C. **(D)** Graphical summary of satellite phenotype frequency observed in all timelapse analysis in (*A*)-(*C*). *n* is number of oocyte meiosis I divisions imaged live. Scale bars in (*A*)-(*C*) are 5 μm. T = 0s for this panel and all panels corresponds to metaphase (see STAR Methods for more detail).

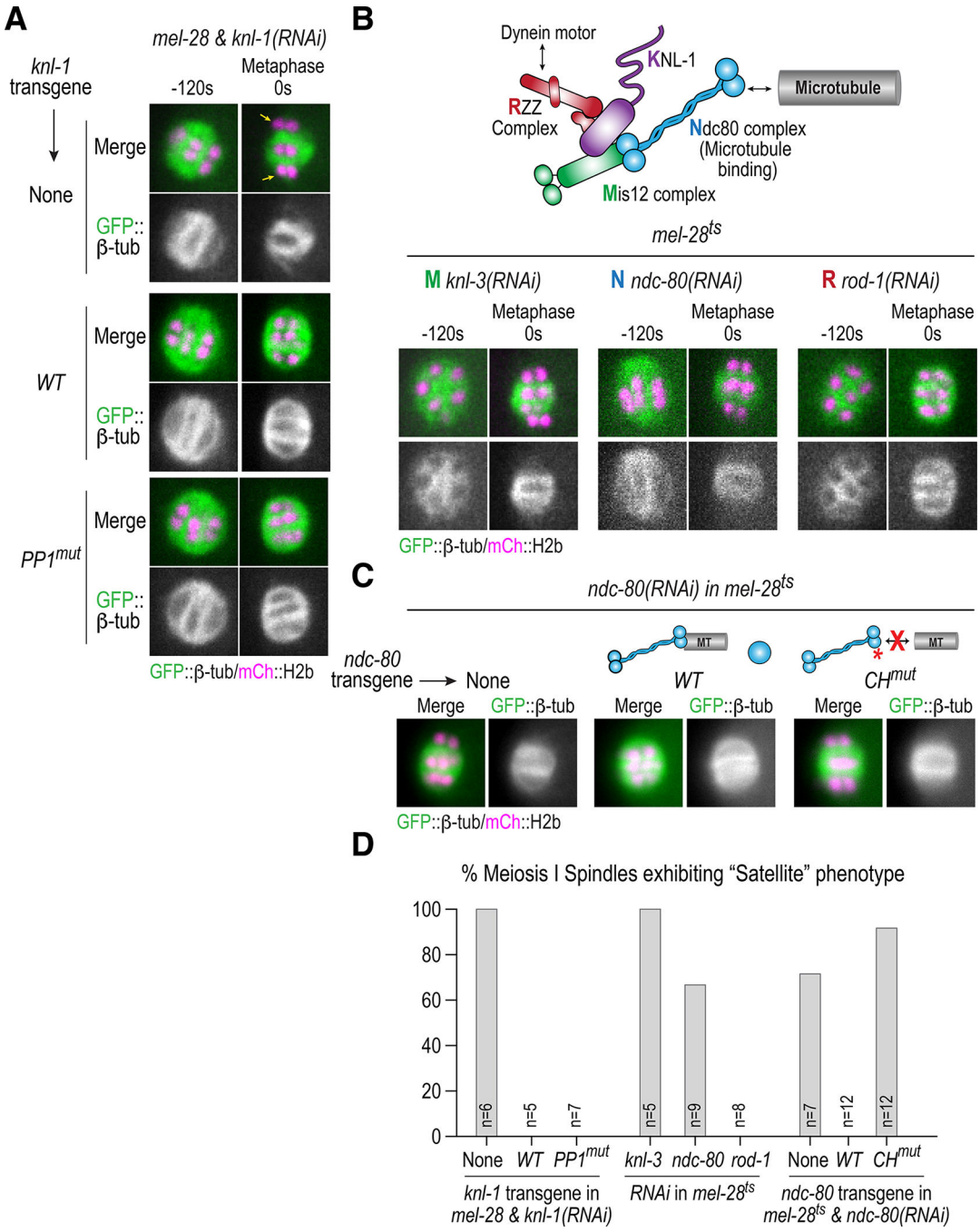

Figure 3. The microtubule-binding activity of the KMN network acts in concert with MEL-28 to keep chromosomes in the oocyte spindle.

(A)–(C) Images from timelapse sequences of the indicated conditions and strains. Transgenes in (*A*) and (*C*) were re-encoded to be RNAi-resistant, enabling replacement of endogenous proteins with transgene-encoded versions. Schematic in (*B*) depicts the molecular composition of the outer kinetochore and panels below show effect of inhibiting a key component of each core complex in a *mel-28*^{ts} mutant strain. **(D)** Graphical summary of satellite phenotype frequency observed in the timelapse analysis in (*A*)-(*C*). *n* is number of

oocyte meiosis I divisions imaged live. Scale bars in (*A*)-(*C*), 5 μm. T = 0s for this panel and all panels corresponds to metaphase (see STAR Methods for more detail).

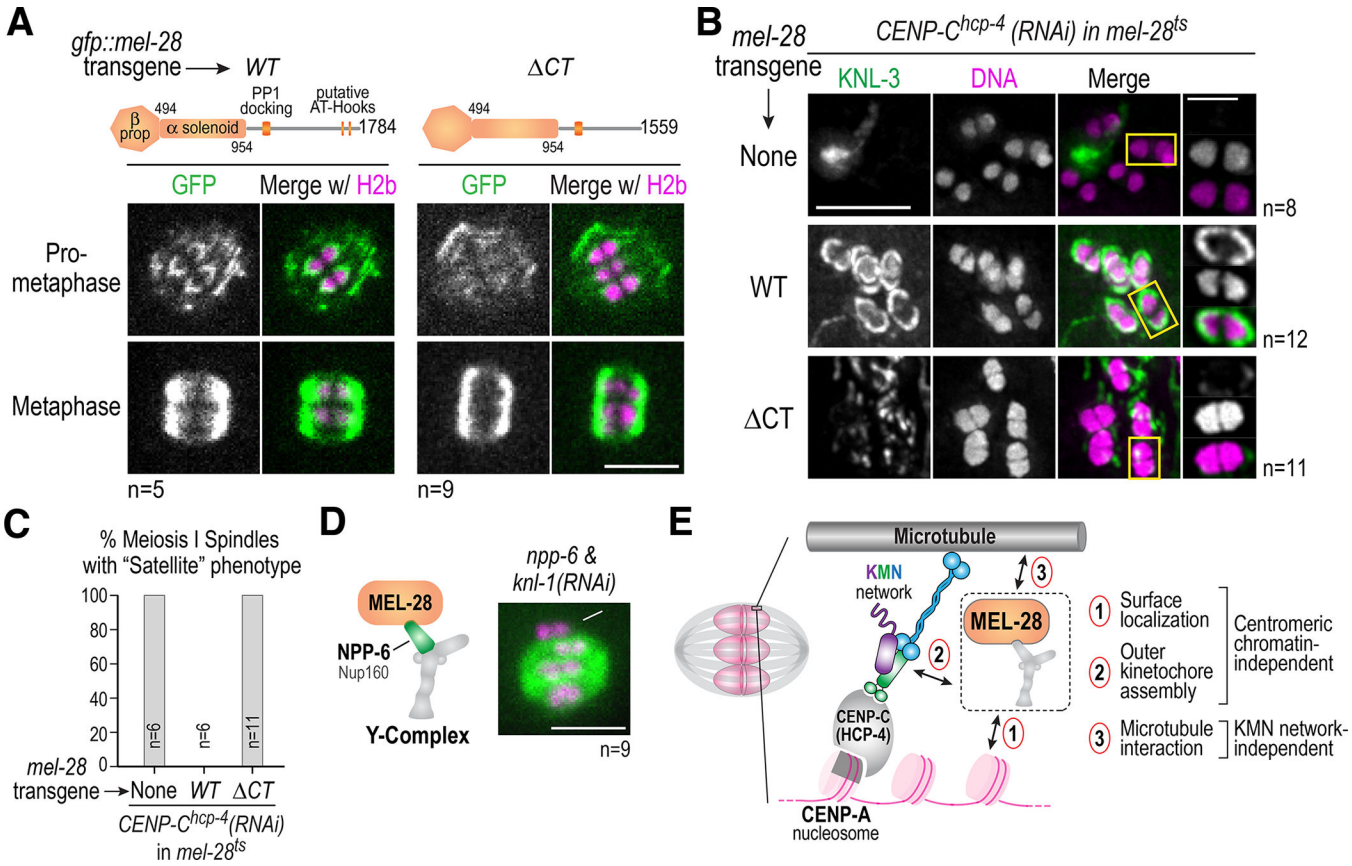

Figure 4. Chromosome surface-localized MEL-28 is important for outer kinetochore assembly and for constraining chromosomes in the oocyte spindle.

(A) Schematics of wild-type (WT) and ΔCT MEL-28 shown above images from timelapse sequences showing GFP::MEL-28 and GFP::MEL-28ΔCT localization in prometaphase and metaphase of meiosis I. Scale bar is 5 μm. **(B)** Immunofluorescence analysis of KNL-3 localization in the indicated conditions. Scale bars are 5 μm (*larger panels*) and 2 μm (*individual chromosomes*). **(C)** Graphical summary of satellite phenotype frequency observed by timelapse analysis in a strain with fluorescently marked chromosomes and microtubules. **(D)** Schematic of MEL-28 association with the core Y-complex and image of a metaphase oocyte meiotic spindle in a NUP160^{NPP-6} and KNL-1 double depletion. The satellite phenotype (*white arrow*) was observed in all 9 double depletion oocytes. For additional images, including of the single NUP160^{NPP-6} depletion, see Figure S3. Scale bar is 5 μm. **(E)** Model highlighting role of MEL-28, and potentially its associated Y-complex, in centromeric chromatin-independent recruitment of the outer kinetochore KMN network to the meiotic chromosome surface, as well as in promotion of chromosome-spindle microtubule interactions in parallel to the KMN network.

Key resources table

REAGENT or RESOURCE	SOURCE	IDENTIFIER
Antibodies		
Rabbit anti-KNL-3	[6]	N/A
Rabbit anti-KNL-1	[40]	N/A
Rabbit anti-NDC-80	[40]	N/A
Rabbit anti-HCP-4	[41]	N/A
Bacterial and virus strains		
E. coli Strain: OP50-1	Caenorhabditis Genetics Center (CGC)	N/A
Experimental models: Organisms/strains		
C. elegans: Strain wild type N2 (ancestral)	CGC	N2
C. elegans: Strain OD3070 *ltIs37 [pAA64; pie-1/mCHERRY::his-58; unc-119 (+)] IV; knl-3(lt46 [gfp::knl-3]) V*	This Study	OD3070
C. elegans: Strain OD4492 *mel-28(ax640) III; ltIs37 [pAA64; pie- 1/mCHERRY::his-58; unc-119 (+)] IV; knl-3(lt46 [gfp::knl-3]) V*	This Study	OD4492
C. elegans: Strain GKC4 *mel-28(ax640) III*	[9]	GKC4
C. elegans: Strain OD868 *ltSi220[pOD1249/pSW077; Pmex-5::GFP-tbb-2-operon-linker-mCherry-his-11; cb-unc-119(+)] I*	This Study	OD868
C. elegans: Strain OD4443 *ltSi220[pOD1249/pSW077; Pmex-5::GFP-tbb-2-operon-linker-mCherry-his-11; cb-unc-119(+)] I; mel-28(ax 640) III*	This Study	OD4443
C. elegans: Strain OD3796 *ltSi220[pOD1249/pSW077; Pmex-5::GFP-tbb-2-operon-linker-mCherry-his-11; cb-unc-119(+)] I; emb-30(tn377) III*	This Study	OD3796
C. elegans: Strain OD2388 *ltSi220[pOD1249/pSW077; Pmex-5::GFP-tbb-2-operon-linker-mCherry-his-11; cb-unc- 119(+)]I;ltSi1[pOD809/pJE110; Pknl-1::KNL-1reencoded::RFP; cb-unc-119(+)]II; unc-119(ed3)III?*	This Study	OD2388
C. elegans: Strain OD3365 *ltSi220[pOD1249/pSW077; Pmex-5::GFP-tbb-2-operon-linker-mCherry-his-11; cb-unc-119(+)] I; ltSi14[pOD857/pJE132; Pknl-1::KNL-1reencoded(RRASA + SAAA mutant)::RFP; cb-unc-119(+)]II*	This Study	OD3365
C. elegans: Strain OD4573 *ltSi220[pOD1249/pSW077; Pmex-5::GFP-tbb-2-operon-linker-mCherry-his-11; cb-unc-119(+)] I; ltSi120[[pDC170;Pndc-80:NDC-80 reencoded; cb-unc-119(+)]II; mel-28(ax640) III*	This Study	OD4573
C. elegans: Strain OD4493 *ltSi220[pOD1249/pSW077; Pmex-5::GFP-tbb-2-operon-linker-mCherry-his-11; cb-unc-119(+)] I; ltSi711[pDC267;Pndc-80:NDC-80(66,96,100,125,144,155AAAAAA) reencoded; cb-unc-119(+)] II; mel-28(ax640) III*	This Study	OD4493
C. elegans: Strain OD1500 *ltSi466[pNH97; Pmel-28::GFP-mel-28 (reencoded exon 14 FL); cb-unc-119(+)] II; ltIs37 [pAA64; pie-1/mCHERRY::his-58; unc-119 (+)] IV*	This Study	OD1500
C. elegans: Strain OD1861 *ltSi596[pNH118; Pmel-28::GFP-mel-28 1-1559 (reencoded exon 14 FL); cb-unc-119(+)] II; ltIs37 [pAA64; pie-1/mCHERRY::his-58; unc-119 (+)] IV*	This Study	OD1861
C. elegans: Strain OD4444 *ltSi220[pOD1249/pSW077; Pmex-5::GFP-tbb-2-operon-linker-mCherry-his-11; cb-unc-119(+)] I; ltSi700[pNH164; Pmel-28::mel-28rr ex14 WT; cb-unc-119(+)] II; mel-28(ax640) III*	This Study	OD4444
C. elegans: Strain OD4446 *ltSi220[pOD1249/pSW077; Pmex-5::GFP-tbb-2-operon-linker-mCherry-his-11; cb-unc-119(+)] I; ltSi1119[pNH286; untagged mel-28 11559 RRexon14::mel-28 3'UTR; cb-unc-119(+)]II; mel-28(ax640) III*	This Study	OD4446
C. elegans: Strain FM348 *aspm-1(or1935[GFP::aspm-1]) I; ltIs37[pAA64; pie-1/mCHERRY::his-58; unc-119 (+)] IV*	[17]	FM348

REAGENT or RESOURCE	SOURCE	IDENTIFIER
C. elegans: Strain OD3192 *klp-19(lt118[gfp::klp-19]) III; unc-119(ed3) III?; ltIs37[pAA64;pie-1/mCHERRY::his58; unc-119(+)] IV*	This Study	OD3192
Oligonucleotides		
Primer 1 for synthesis of dsRNA targeting *mel-28(C38D4.3)*: taatacgactcactataggAGAAATACTCGATCCGCATC; Template: N2 Genomic DNA	This Study	N/A
Primer 2 for synthesis of dsRNA targeting *mel-28(C38D4.3)*: aattaaccctcactaaaggAGTTACACTTCCAGCTCTAC; Template: N2 Genomic DNA	This Study	N/A
Primer 1 for synthesis of dsRNA targeting *mel-28* (*C38D4.3*) for KLP-19 localization analysis: aattaaccctcactaaaggCGTGTCCTGGATGTTCT GG; Template: N2 Genomic DNA	This Study	N/A
Primer 2 for synthesis of dsRNA targeting *mel-28* (*C38D4.3*) for KLP-19 localization analysis: taatacgactcactataggTTTATCGATGGGAGGCATTC; Template: N2 Genomic DNA	This Study	N/A
Primer 1 for synthesis of dsRNA targeting *hcp-4(T03F1.9)*: aattaaccctcactaaaggGGAAATGTACGGAGCGAAAA; Template: N2 Genomic DNA	This Study	N/A
Primer 2 for synthesis of dsRNA targeting *hcp-4(T03F1.9)*: taatacgactcactataggACATTGTTGGTGGGTCCAAT; Template: N2 Genomic DNA	This Study	N/A
Primer 1 for synthesis of dsRNA targeting *knl-1(C02F5.1)*: taatacgactcactataggAACAACCATGTGAGGCTGGT; Template: N2 Genomic DNA	This Study	N/A
Primer 2 for synthesis of dsRNA targeting *knl-1(C02F5.1)*: aattaaccctcactaaaggGCGCCAGTATTCGAGGTATC; Template: N2 Genomic DNA	This Study	N/A
Primer 1 for synthesis of dsRNA targeting *ndc-80(W01B6.9)*: aattaaccctcactaaaggGATGACAAGTACATTCAGAGATTATACAAATGATC; Template: N2 cDNA	This Study	N/A
Primer 2 for synthesis of dsRNA targeting *ndc-80(W01B6.9)*: taatacgactcactataggGTGGTTCAAGATTCATTTGAATATTAAGTCCACTG; Template: N2 cDNA	This Study	N/A
Primer 1 for synthesis of dsRNA targeting *rod-1(F55G1.4)*: aattaaccctcactaaaggAATGCAAATCTTTTTGGATGGGAGAAAC; Template: N2 Genomic DNA	This Study	N/A
Primer 2 for synthesis of dsRNA targeting *rod-1(F55G1.4)*: taatacgactcactataggCATCGACGAATTTGATTCGATCAATC; Template: N2 Genomic DNA	This Study	N/A
Primer 1 for synthesis of dsRNA targeting *knl-3(T10B5.6)*: taatacgactcactataggGTCGAGAAAACTTCCGTGAAG; Template: N2 Genomic DNA	This Study	N/A
Primer 2 for synthesis of dsRNA targeting *knl-3(T10B5.6)*: aattaaccctcactaaaggATGTCTCAAAAATCAAACGACACC; Template: N2 Genomic DNA	This Study	N/A
Primer 1 for synthesis of dsRNA targeting *npp-6* (F56A3.3): taatacgactcactataggATTGTCGTTCCCACAGCTTC; Template: N2 Genomic DNA	This Study	N/A
Primer 2 for synthesis of dsRNA targeting *npp-6* (F56A3.3): aattaaccctcactaaaggTATTGCCGATCGGTTCTTCT; Template: N2 Genomic DNA	This Study	N/A
Recombinant DNA		
Plasmid for GFP::KLP-19 CRISPR Tagging: pDD162	[44]	Addgene_47549
Plasmid for GFP::KLP-19 CRISPR Tagging: pCFJ90 [Pmyo-2::mCherry (pharynx muscle)]	[45]	Addgene_19327
Plasmid for GFP::KLP-19 CRISPR Tagging: pCFJ104 [Pmyo-3::mCherry (body muscle)]	[45]	Addgene_19328
Plasmid for GFP::KLP-19 CRISPR Tagging: pGH8 [Prab-3::mCherry (pan-neuronal)]	[45]	Addgene_19359
Software and algorithms		
Fiji	[43]	SCR_002285
Prism	GraphPad	SCR_002798
Adobe Illustrator	Adobe	SCR_010279
Other		